Polymer Chemistry

PAPER

View Article Online
View Journal | View Issue

Published on 18 December 2013. Downloaded by Fudan University on 21/01/2018 11:51:09.

Cite this: *Polym. Chem.*, 2014, **5**, 2592

The precise molecular location of gadolinium atoms has a significant influence on the efficacy of nanoparticulate MRI positive contrast agents†

Yang Li,[a] Sophie Laurent,[b] Lars Esser,[de] Luce Vander Elst,[b] Robert N. Muller,[bc] Andrew B. Lowe,*[d] Cyrille Boyer*[ad] and Thomas P. Davis*[ef]

Received 3rd December 2013
Accepted 18th December 2013

DOI: 10.1039/c3py01676e

www.rsc.org/polymers

In this work, we studied the influence of the structure of macromolecular ligands on the relaxivity of gadolinium contrast agents constructed as nanoparticle systems. Macromolecular ligands were assembled as single-molecule nanoparticles in the form of either discrete core cross-linked star polymers or hyperbranched polymers. 1-(5-Amino-3-aza-2-oxypentyl)-4,7,10-tris(*tert*-butoxycarbonylmethyl)-1,4,7,10-tetraaza-cyclododecane (DO3A–*t*Bu–NH_2) chelate was incorporated into different parts (arms, cores, and end-groups) of the polymeric structures using activated ester/amine nucleophilic substitutions, deprotected and complexed with Gd^{3+}. The relaxivity properties of the ligated Gd^{3+} agents were then studied to evaluate the effect of macromolecular architecture and Gd^{3+} placement on their behavior as discrete nanoparticle magnetic resonance imaging (MRI) contrast agents. The precise placement of Gd^{3+} in the polymeric structures (and therefore in the nanoparticles) proved to be critical in optimizing the performance of the nanoparticles as MRI contrast agents. The relaxivity was measured to vary from 11 to 22 mM^{-1} s^{-1}, 2–5 times higher than that of a commercial DOTA–Gd contrast agent when using a magnetic field strength of 0.47 T. The relaxivity of these nanoparticles was examined at different magnetic fields from 0.47 T to 9.4 T. Finally, the residence time of the coordinated water (τ_M) and the rotational correlation time of the final molecule (τ_R) were evaluated for these different nanostructures and correlated with the polymeric architecture.

Introduction

Magnetic Resonance Imaging (MRI) is an indispensable clinical tool used for the early detection of diseases with widespread applications in cancer and cardiovascular diagnosis. MRI is a non-invasive technique, exhibiting excellent spatial and temporal resolution whilst obviating exposure to harmful radiation. However, the sensitivity of MRI to differences in tissue type is relatively low. To overcome this lack of sensitivity, contrast agents (CAs) are usually administered to the patient prior to the MRI procedure. The contrast agent enters the circulation system and serves to shorten the longitudinal (T_1) or transversal (T_2) relaxation times of surrounding water protons (under an applied magnetic field). Two broad categories of CAs for MRI exist: (1) positive (or T_1) contrast agents that mainly shorten T_1 and give rise to image brightening, these are most commonly paramagnetic gadolinium based CAs[1–3] or (2) negative (or T_2) contrast agents that largely decrease T_2 leading to image darkening; superparamagnetic iron nanoparticles being the most important example.[4–10] Positive contrast agents based on low molecular weight Gd^{3+} chelates, namely Gd–diethylenetriaminepentaacetic acid (Gd–DTPA) or Gd–tetraazacyclododecanetetraacetic acid (Gd–DOTA), exist as commercial products and are routinely employed in clinical settings.[3,11,12] New, higher magnetic field (3.0 T) MRI scanners have entered the market, providing improved image resolution and detection limits. The currently used commercial (low molecular weight) CAs have an inadequate performance at higher magnetic fields leading to a significant decrease in image contrast. Currently, to overcome this contrast problem at higher field strengths, clinicians need to increase the concentration of Gd^{3+} to offset the relaxivity decrease. An increase in Gd^{3+} contrast agent is seen to be undesirable both from a cost and a safety viewpoint as any Gd^{3+} leakage and/or systemic accumulation can (in a small

[a]*Australian Centre for Nanomedicine (ACN), School of Chemical Engineering, The University of New South Wales, Sydney, NSW 2052, Australia. E-mail: cboyer@unsw.edu.au*

[b]*NMR and Molecular Imaging Laboratory, Department of General, Organic and Biomedical Chemistry, University of Mons, 7000 Mons, Belgium*

[c]*CMMI – Center of Microscopy and Molecular Imaging, Rue Adrienne Bolland 8, B-6041 Gosselies, Belgium*

[d]*Centre for Advanced Macromolecular Design, School of Chemical Engineering, University of New South Wales, Kensington, Sydney, NSW 2052, Australia. E-mail: a.lowe@unsw.edu.au*

[e]*Monash Institute of Pharmaceutical Sciences, Monash University, Parkville, VIC 3052, Australia. E-mail: thomas.p.davis@monash.edu*

[f]*Department of Chemistry, University of Warwick, Coventry, CV4 7AL, UK*

† Electronic supplementary information (ESI) available. See DOI: 10.1039/c3py01676e

This journal is © The Royal Society of Chemistry 2014

Published on 18 December 2013. Downloaded by Fudan University on 21/01/2018 11:51:09.

minority of cases) cause nephrogenic systemic fibrosis.[13] Previous work has shown that nanoparticles can have advantages as CAs because each nanoparticle structure can incorporate multiple Gd^{3+} ions enhancing contrast *via* both a concentration effect and by reducing molecular tumbling[14–17] leading to a significant shortening of relaxation times and, consequently, an enhancement of contrast (potentially permitting reduced clinical dosing).[18–20] Additionally, a nanoparticle structure can provide a scaffold to attach tissue-specific targeting moieties (multiple sites favouring the multi-ligand effect), which could be potentially used to enhance specific Gd^{3+} concentration at diseased tissue sites. In previous work, Gd^{3+} chelates have been covalently bound to biocompatible linear polymers (*e.g.* poly(lysine)[21] or poly(*N*-(2-hydroxypropyl)methacrylamide)[22]) and also to complex structures, such as block copolymer micelles[23–27] or dendrimers.[28–30] In very recent publications, polymeric CAs based on core cross-linked star (CCS) and hyperbranched (HBP) architectures were reported both by Adkins and co-workers[31] and by us.[32] In the approach described by Adkins and co-workers, catechol chelates were attached to the arms of star molecules yielding CAs with a very high relaxivity (84 mM^{-1} s^{-1}). In our initial study, we demonstrated the loading of multiple Gd^{3+} ions into single macromolecular chains yielding efficient macromolecular positive contrast agents. The purpose of the present communication was to investigate the influence of the precise molecular placement of Gd^{3+} ions within nanoparticles on MRI relaxivity (r_1).

Results and discussion

Core cross-linked star polymers (CCS) and hyperbranched polymers (HBPs) consist of single macromolecular chain structures built to form 3D tertiary structures by cross-linking and branching. CCS and HBP can form discrete nanoparticle structures useful in a wide range of applications.[33–40] In the present work, three different CCS polymers and two HBPs were prepared using reversible addition–fragmentation chain transfer (RAFT) polymerization[41,42] of oligo(ethyleneglycol methyl ether) acrylate (OEGA) in the presence of a cross-linker and an activated ester monomer: pentafluorophenyl acrylate (PFPA). The activated ester groups in the polymeric architecture were subsequently exploited to attach a common chelating agent (DO3A). The position of activated ester groups was varied in each different polymer structure, allowing the placement of the chelating agent in each macromolecular chain to be changed, as shown in Scheme 1. The CCS were prepared using a degradable cross-linker based on disulfide with the aim of imparting intracellular biodegradability to the nanoparticles to aid bioelimination in future *in vivo* studies; disulfide bonds can be easily reduced (broken) in the presence of glutathione[43] thereby breaking the nanoparticles down to lower molecular weight linear chains (Fig. S1–S17 in the ESI†).

Synthesis of core cross-linked nanogel star (CCS) polymers

CCS polymers were synthesized using an arm first approach as reported previously (Fig. S1 in the ESI†).[44,45] Three different

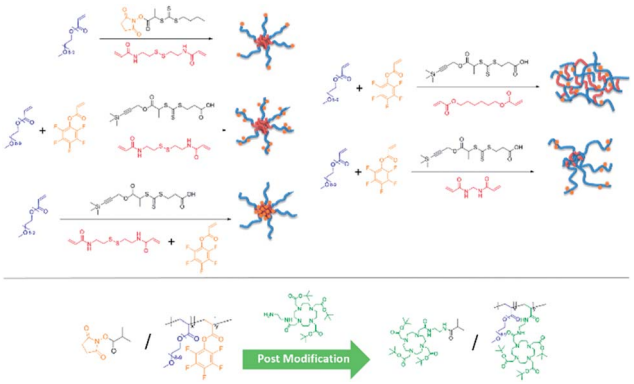

Scheme 1 Synthesis of polymeric contrast agents.

polymer arms were synthesized using two different RAFT agents. Table 1 lists the different polymers that were prepared.

Synthesis of core cross-linked star A. In CCS-A, the activated ester groups were incorporated at the termini of the polymer arms (the star periphery) using a NHS functionalized RAFT agent.[46] The NHS-RAFT agent (Fig. S2 and S3 in the ESI†) was used to control the polymerization of OEGA in the presence of AIBN as an initiator at 65 °C, yielding NHS-terminal OEGA. The polymer was purified and then characterized by NMR and SEC analyses. SEC analysis confirmed the successful synthesis of OEGA polymers with low dispersities (D_m < 1.20). ^{1}H NMR analysis (Fig. S4 in the ESI†) confirmed the presence of terminal NHS groups by the presence of a signal at 2.9 ppm, which was then employed to calculate the molecular weight of the chains *via* the following equation: $\bar{M}_{n,NMR} = [I^{at\ 3.3\ ppm}/(3 \times I^{at\ 2.9})] \times M_w^{OEGA} + M_w^{RAFT}$, with $I^{at\ 3.3\ ppm}$ and $I^{at\ 2.9\ ppm}$ corresponding to the integration of signals at 3.3 ppm and 2.9 ppm. The theoretical molecular weight values were in accord with the experimental molecular weights obtained using SEC and NMR analyses. Subsequently, the NHS-OEGA was chain extended and cross-linked to form stars (using a $[P(OEGA)]_0$: $[Cross\text{-}linker]_0$ ratio of 1 : 8).

Synthesis of core cross-linked star B (CCS-B). In CCS-B, the activated ester (PFP) groups were incorporated into the polymer arms as follows: copolymerization reactions of PFPA and OEGA were performed to yield linear poly(OEGA-*co*-PFPA) copolymers with a molar feed ratio of 70 mol% OEGA (Fig. S5 and S6 in the ESI†). Using ^{19}F NMR analyses confirmed that the final compositions of the copolymer corresponded to the initial monomer feed ratios (Table 1). The polymerization reactions were controlled by the RAFT process as evidenced by the close accord of experimental and theoretical $\bar{M}_n$ values ($\bar{M}_{n,theo}$ = 11 000 g mol^{-1}, calculated from the following equation: $\bar{M}_{n,theo} = (\alpha^{OEGA} \times [OEGA]_0/[RAFT]_0 \times M_w^{OEGA}) + (\alpha^{PFPA} \times [PFPA]_0/[RAFT]_0 \times M_w^{PFPA}) + M_w^{RAFT}$, with $[OEGA]_0$, $[PFPA]_0$ and $[RAFT]_0$ corresponding to the initial concentrations of OEGA, PFPA and RAFT agents respectively). The copolymer chains all had relatively low dispersity values as determined by SEC (Fig. S1 in the ESI†). Subsequently, all copolymers were chain extended in the presence of a disulfide cross-linker to yield CCS-B (using a $[P(OEGA\text{-}co\text{-}PFPA)]_0$: $[cross\text{-}linker]_0$ ratio of 1 : 8).

Published on 18 December 2013. Downloaded by Fudan University on 21/01/2018 11:51:09.

Table 1 Characteristics of different star arms[a]

Arms	$\bar{M}_{n,SEC}$[b] (g mol^{-1})	$\bar{M}_{n,NMR}$[c] (g mol^{-1})	$Đ_m$[b]	F_{OEGA}[d,e]	F_{AE}[d,e]	f_{OEGA}[c,e]	f_{AE}[c,e]
Arm-A	10 000	9800	1.16	97	3*	89	11*
Arm-B	9000	8900	1.14	78	22**	80	20**
Arm-C	11 000	10 700	1.14	100	0	100	0

[a] AE: activated ester, * NHS active ester and ** pentafluorophenyl ester. [b] Assessed by SEC in DMAC (0.03% w/v LiBr, 0.05% BHT) using a conventional calibration curve with narrow molecular weight distribution PS standards. [c] Assessed by ^{1}H NMR in $CDCl_3$ and calculated by conversion and composition. [d] Initial feed molar composition (%). [e] Molar composition (%).

Synthesis of core cross-linked star C (CCS-C). In CCS-C, the activated ester (PFP) groups were incorporated into the star cores as follows: an OEGA homopolymer with $\bar{M}_n$ = 10 000 g mol^{-1} was prepared by the RAFT polymerization of OEGA at 60 °C over 12 h using AIBN as an initiator and 3-(trimethylsilyl)-prop-2-yn-1-yl 2-((((3-propionic acid)thio)carbonothioyl)thio) propanoate as the CTA. OEGA was then used as a macroCTA to control the copolymerization of PFPA in the presence of a cross-linker, *N*,*N*′-bis(acryloyl)cystamine in toluene at 70 °C for 24 h, with a $[PFPA]_0 : [cross\text{-}linker]_0 : [OEGA]_0$ ratio of 30 : 8 : 1. We demonstrated previously[44,47] that under reaction conditions where the cross-linker is only partially soluble in the polymerization solvent (toluene in this case) a high incorporation of arms occurs yielding low dispersity CCS polymers. ^{19}F NMR analyses were used to confirm the presence of pentafluorophenyl ester (PFP) groups in the polymer chains as evidenced by the presence of signals at −152.5, −156.0 and −162.5 ppm (Fig. S8 in the ESI†). The precise composition of PFP groups in the star polymers was calculated using 2,2,2-trifluoroethanol as a reference (see ESI† for details). The final concentration of PFP groups was found to correspond to the expected composition based on the monomer feed, see Table 2.

Characterization of core cross-linked nanogel star (CCS) polymers

Unpurified CCSs were analyzed by SEC to determine the efficiency of arm-polymer incorporation within the star structures and also to determine the molecular weights and $Đ_m$s of the resultant star polymers (Fig. 1A–C). All the star polymers manifested low $Đ_m$s (less than 1.20), as shown in Table 2. The CCSs were purified, removing any excess arm polymer, by precipitation in a mixture of diethyl ether and dichloromethane (DCM). SEC analyses were performed after confirming arm removal and retention of the narrow star molecular weight distributions (Fig. S1 in the ESI†). In addition, using the molecular weight data obtained by SEC, we estimated the number of arms on each star from the following equation: $N^{arms} = \bar{M}_n^{CCS}/\bar{M}_n^{Arm}$, where $\bar{M}_n^{CCS}$ and $\bar{M}_n^{Arm}$ correspond to the molecular weights of CCS and the arms; the CCS structures were found to contain ~6 arms. Using ^{19}F NMR and ^{1}H NMR analyses, we were able to determine the concentrations of PFP and NHS groups present in the CCS polymers (data shown in Table 2). The nanoparticles typically exhibit a size of around 15 nm with CCS nanoparticles (A, B and C) in water determined by dynamic light scattering (DLS) with low dispersities (0.1, measured by DLS) (Fig. 1D).

Synthesis of hyperbranched P(OEGA-*co*-PFPA) copolymers

A one-pot procedure was employed to synthesize the hyperbranched polymers.[48–50] *N*,*N*′-Methylenebisacrylamide and 1,6-hexanediol diacrylate were chosen as cross-linkers. Copolymerization reactions with a monomer feed ratio of 12.8 : 3.3 : 1.6 : 1.0 ($[OEGA]_0/[PFPA]_0/[Cross\text{-}linker]_0/[RAFT]_0$) were carried out at 60 °C for 24 h yielding hyperbranched polymers. The conversions of PFPA, OEGA and cross-linker were monitored using ^{1}H and ^{19}F NMR analyses (see ESI† for calculation). Fig. 2 shows the monomer conversions for the syntheses of hyperbranched polymers made using the two different cross-linkers. The kinetics of

Table 2 Characteristics of core cross-linked nanogel star (CCS) polymers and hyperbranched polymers (HBP)

	$\bar{M}_{n,SEC}$[a] (g mol^{-1})	$Đ_m$[a]	Size[b] (nm)	$\bar{M}_{n,SEC}$[a] of arm (g mol^{-1})	N^{arms}[c]	F_{OEGA}[d] (%)	F_{PFP}[d] (%)	F_{NHS}[d] (%)	f_{OEGA}[d] (%)	f_{DO3A}[d] (%)	N^{Gd}[e]	N^{Gd}[f]
CCS-A	58 000	1.12	11	10 000	6	89	—	11	89	11	6	6
CCS-B	56 000	1.09	10	9000	6	80	20	—	80	20	63	60
CCS-C	68 000	1.14	11	11 000	6	60	40	—	58	38	150	133
HBP-D	34 000	1.53	9	—	—	75	25	—	75	25	47	45
HBP-E	39 000	3.71	10	—	—	76	24	—	73	23	52	50

[a] Assessed by SEC in DMAC (0.03% w/v LiBr, 0.05% BHT) using a conventional calibration curve with narrow PS standards. [b] Assessed by DLS in water and counted by intensity. [c] Number of arms on each star from the following equation: $N^{arms} = \bar{M}_n^{CCS}/\bar{M}_n^{Arm}$, where $\bar{M}_n^{CCS}$ and $\bar{M}_n^{Arm}$ correspond to the molecular weights of CCS and the arms. [d] Molar composition (%) assessed by ^{1}H NMR in $CDCl_3$. [e] Theoretical values of Gd^{3+} calculated with the assumption that one DO3A contained one Gd^{3+}. [f] Number of gadolinium atoms per macromolecule (N^{Gd}) calculated by N^{Gd} = ([Gd content]/$\bar{M}_w^{Gd}$)/([polymer content]/$\bar{M}_n^{polymer}$), with Gd content, $\bar{M}_w^{Gd}$ and $\bar{M}_n^{polymer}$ correspond to the Gd content assessed by ICP-MS, molar mass of Gd, and molecular weight of polymer.

 This journal is © The Royal Society of Chemistry 2014

Published on 18 December 2013. Downloaded by Fudan University on 21/01/2018 11:51:09.

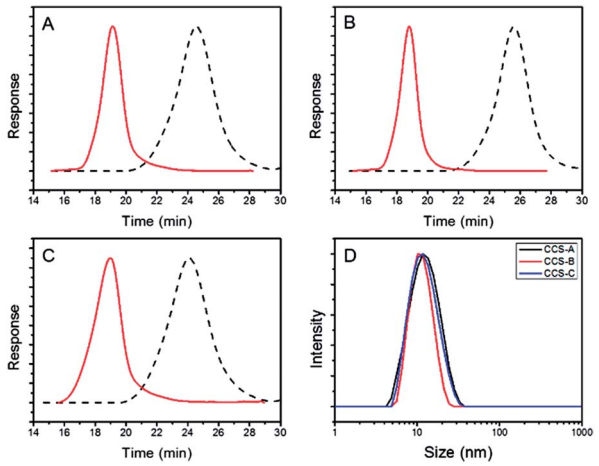

Fig. 1 SEC traces (A, CCS-A; B, CCS-B; C, CCS-C) of CCS (—) and star arm (-·-) and DLS measurements of different CCS (D).

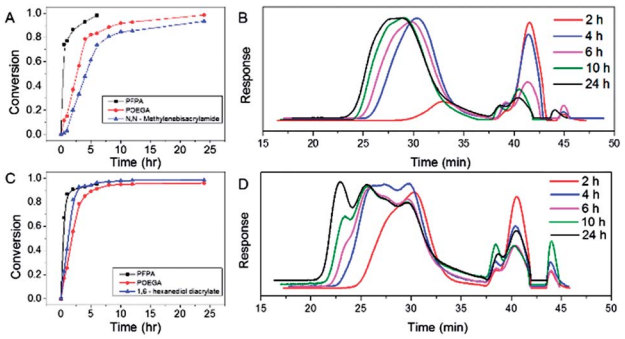

Fig. 2 (A and C) PFPA, OEGA and cross-linker conversions *versus* time; and SEC traces of the hyperbranched polymer synthesized using (B) *N*,*N*′-methylenebisacrylamide and (D) 1,6-hexanediol diacrylate, respectively.

the cross-linking reactions differed with 1,6-hexanediol diacrylate polymerizing faster than *N*,*N*′-methylenebisacrylamide according to the different reactivities of the two cross-linkers resulting in slightly different hyperbranched structures.

Hyperbranched polymers (HBP-D) made using *N*,*N*′-methylenebisacrylamide as a cross-linker

In the terpolymerization of PFPA, *N*,*N*′-methylenebisacrylamide, OEGA, the PFPA initially polymerized preferentially, resulting in PFPA chain enrichment, and a monomer concentration gradient within the chains as polymerization progressed, with the cross-linker functionality preferentially incorporated later in the polymerization, resulting in specific structures as shown in Scheme 2. SEC traces of the hyperbranched polymers indicated mononodal but non-symmetric distributions with $Đ_m$s < 1.6 (Fig. 2C) and multimodal molecular weight distributions when *N*,*N*′-methylenebisacrylamide and 1,6-hexanediol diacrylate were employed respectively.

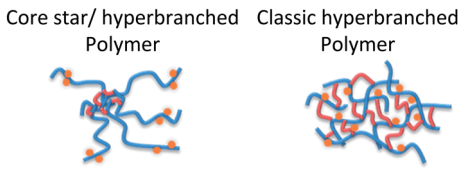

Scheme 2 Schematic structures of hyperbranched polymers synthesized using *N*,*N*′-methylenebisacrylamide and 1,6-hexanediol diacrylate, respectively.

Hyperbranched polymers (HBP-E) made using 1,6-hexanediol diacrylate as a cross-linker

In the terpolymerization with 1,6-hexanediol diacrylate, as before the PFPA polymerized faster than the other monomers, but in this case the cross-linker was incorporated more evenly throughout the chain reaction. In this case, we can envisage a slightly different hyperbranched structure, as shown in Scheme 2. SEC analyses confirmed the formation of hyperbranched polymers with broad molecular weight distributions (Fig. 2). Both hyperbranched polymer structures were easily re-dispersed in water, forming discrete nanoparticles with typical sizes of 10 nm (determined by DLS).

DO3A post-modification of CCS and HBP polymers

The activated ester groups (PFP or NHS) were used to attach the DO3A chelating agent to the different tertiary structures. The ligand–modification reactions were carried out with a slight excess of the *N*-(2-propionamidoethyl)amine derivative of the chelate tri-*tert*-butyl-2,2′,2″-(1,4,7,10-tetraazacyclododecane-1,4,7-triyl)triacetate (DO3A-*t*Bu) in DMF for 48 h at room temperature (using a ratio $[PFP/NHS]_0 : [DO3A]_0 = 1 : 1.1$). Subsequently, FT-IR spectroscopy confirmed the absence of absorptions at 1780 cm^{-1} and 1770 cm^{-1} for PFP and NHS respectively, after reaction with DO3A. The successful reaction of PFP activated ester groups was also confirmed by the absence of ^{19}F NMR signals at −152, −157 and −162 ppm (Fig. S18–S22 in the ESI†). ^1H NMR spectroscopy was also used to confirm the successful attachment of DO3A, as evidenced by a new signal at 1.4 ppm arising from the *tert*-butyl groups associated with DO3A–*t*Bu–NH_2 (see ESI†). The number of DO3A, calculated using the following equation: $f^{DO3A} = I^{1.4–1.7\ ppm}/27/[(I^{4.1–4.2\ ppm}/2) + (I^{1.4–1.7\ ppm}/27)]$ with $I^{1.4–1.7\ ppm}$ and $I^{4.1–4.2\ ppm}$, correspond to the integrals of *tert*-butyl group and CH_2 ester group, respectively, attached to the polymeric nanoparticles, in good accord with the number of activated ester groups incorporated into the polymeric nanoparticles.

Subsequently, the *tert*-butyl groups were successfully cleaved using trifluoroacetic acid (TFA). CCS and HBP polymers were incubated with Gd^{3+} for 48 h at pH = 8.0. After careful purification *via* dialysis against water for several days (until free Gd^{3+} was completely absent), XPS confirmed that Gd^{3+} was encapsulated into DO3A by the presence of a Gd^{3+} binding energy at 143 eV (data not shown). The amounts of Gd^{3+} encapsulated into the polymer nanostructures were determined by ICP-OES, as given in Table 2. The amounts of Gd measured to be encapsulated were completely consistent with theoretical calculations based on 1 : 1 stoichiometry. The different

Published on 18 December 2013. Downloaded by Fudan University on 21/01/2018 11:51:09.

nanostructures could each encapsulate from 6 to 133 Gd^{3+} ions. The sizes of the nanoparticles were determined by DLS in water, with sizes measured of 9–12 nm.

Relaxometric studies

The improvement in contrast induced by MRI positive CAs is generally represented by the relaxivity (r_1), defined as:

$$r_1 = \frac{1}{[Gd^{3+}]} \times \left(\frac{1}{T_{1,obs}} - \frac{1}{T_{1,H_2O}} \right) \quad (1)$$

where $[Gd^{3+}]$ is the concentration of Gd^{3+} in mM and $T_{1,obs}$ and T_{1,H_2O} are the longitudinal relaxation times in the presence and absence of the MRI CA respectively. The relaxivity value depends on various factors including the external field strength, the number of coordinated water molecules, water exchange rate, rotational diffusion, first and second coordination sphere hydration, and the ion to water proton distance.[18] DOTA-like chelates, such as the DO3A-monoamide used in this work, have a single water molecule coordinated to the Gd^{3+} ion.[18] Critical parameters such as the residence time of the coordinated water (τ_M) and the rotational correlation time of the final molecule (τ_R) are most influential in determining contrast efficacy when attaching CAs to a nanoparticle structure (Scheme 3).[51] Ideally, for small organic contrast agents, τ_M should be at maximum 10 ns and τ_R should be higher than 10 ns in a magnetic field of 1.5 T (most commonly used in MRI scanners).[1,52]

The results obtained following relaxometric studies at 0.47, 1.41 and 9.4 T (37 °C) using the P(OEGA-*co*-DO3A-MA-Gd^{3+}) nanoparticle contrast agents with different Gd^{3+} placement are reported in Table 3. The values of r_1 indicated an overall increase in relaxivity compared to the relaxivity of free (non-nanoparticles) DO3A–NH_2–Gd^{3+} (5.2 mM^{-1} s^{-1}) at 0.47 T at 25 °C.[53] The increase in relaxivity is highest for the hyperbranched and CCS-A polymer architectures, with measured relaxivities three/four times higher than for the free chelate (Table 3).

At low magnetic field strength (0.47 T), CCS-C has the lowest relaxivity whilst the highest relaxivity was observed for CCS-A, which exhibits a relaxivity comparable to Gd-decorated dendrimers,[28] with a five-fold increase in the relaxivity over values obtained when using a commercial contrast agent (Magnevist). The rigid nanoparticle structure imposes isotropic rotational dynamic restrictions, increasing τ_R and yielding ionic r_1 values in the order of several tens of mM^{-1} s^{-1}.[20,54] Interestingly, Gd-nanoparticles constructed from both HBP polymers (D and E) induce the same relaxivity at 0.47 T, independent of any differences in their molecular chain structures. The relaxivities obtained for HBP (D and E) are quite similar to the relaxivity induced by CCS-B (Gd in the star arms). At a clinical field strength (1.41 T), the r_1 relaxivity of CCS-A decreased to 15.6 mM^{-1} s^{-1}, while, in contrast, the other nanostructures were less strongly affected. Measurements taken at 9.4 T showed a further decline in induced relaxivity, r_1, for all the nanostructures. Caravan *et al.*[3] demonstrated that the relaxivity r_1 of Gd decreases with magnetic strength and a maximum calculated relaxivity value for Gd^{3+} is around 18 mM^{-1} s^{-1} at 9.4 T. Fig. 3 shows the nuclear magnetic field relaxation dispersion (NMRD) profiles of the various nanoparticulate CAs. A maximum in relaxivity was observed for all the nanoparticle architectures at 40 MHz, within the magnetic field range (12.5 MHz to 125 MHz) used in clinical MRI scanners.

To better understand the differences in the mechanism of action of the CCS and HBP nanoparticles, nuclear magnetic relaxation dispersion (NMRD) profiles were analysed using the usual theoretical model including the innersphere contribution (IS) described by the Solomon–Bloembergen–Morgan equations,[55] the outersphere contribution (OS) and when necessary a second sphere contribution (SS) was taken into account (Fig. S33 in the ESI†). The 'best-fit' parameters are given in Table 4.

Table 3 Relaxivity values for core cross-linked star polymers and hyperbranched polymers

	0.47 T (mM^{-1} s^{-1})	1.41 T (mM^{-1} s^{-1})	9.4 T (mM^{-1} s^{-1})
CCS-A	21.57	15.63	4.71
CCS-B	15.86	13.28	4.81
CCS-C	11.12	9.98	5.16
HBP-D	17.08	14.71	4.25
HBP-E	17.17	14.76	4.41

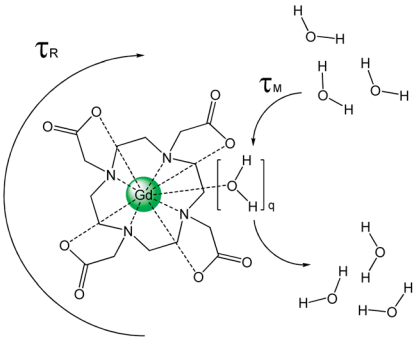

Scheme 3 Different parameters affecting the relaxivity of Gd^{3+} in water, q, τ_M and τ_R correspond to the number of water molecules coordinated to Gd^{3+}, water residency time and the rotational correlation time of the final molecule, respectively.

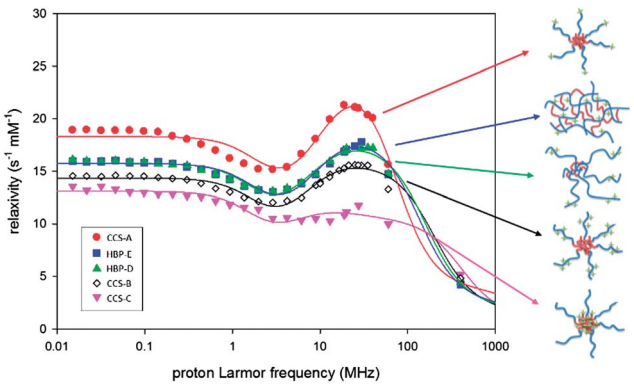

Fig. 3 ^1H NMRD profiles of P(OEGA-*co*-DO3A-MA-Gd^{3+}) with various architectures.

This journal is © The Royal Society of Chemistry 2014

Published on 18 December 2013. Downloaded by Fudan University on 21/01/2018 11:51:09.

Table 4 Values of the parameters obtained from the fittings of the NMRD curves[a]

	τ_R (ns)	τ_M (ns)	τ_{SO} (ps)	τ_V (ps)	τ_{SS} (ps)	q_{SS}
CCS-A	7.7 ± 0.7	891 ± 13.5	155 ± 2	38.9 ± 1.1	70 ± 1.2	2.73 ± 0.04
	7.49 ± 0.7*	896 ± 11.4*	156 ± 6.0*	39.2 ± 1.3*	69.1 ± 1.3*	2.75 ± 0.11*
CCS-B	1.47 ± 0.03	986 ± 14.8	184 ± 2.1	39.8 ± 0.4	70 ± 0.3	0.76 ± 0.02
	1.28 ± 0.04*	900 ± 14.3*	195 ± 9.1*	39.4 ± 2.0*	42.8 ± 19.5*	0.73 ± 0.36*
	1.37 ± 0.04**	900 ± 13.7**	248 ± 4.7**	40.3 ± 1.6**		
CCS-C	0.55 ± 0.02	1000 ± 3.7	251 ± 5.7	43.4 ± 3.4		
	0.47 ± 0.01**	900 ± 3.3**	235 ± 5.4**	49.7 ± 4.0**		
HBP-D	2.03 ± 0.04	936 ± 17.4	189 ± 4.1	36 ± 1.5	32.1 ± 4.9	2.15 ± 0.32
	1.85 ± 0.07*	899 ± 0.1*	208 ± 7.8*	39.1 ± 1.8*	52.2 ± 12.4*	1.09 ± 0.18*
	1.32 ± 0.05**	753 ± 26.4**	270 ± 7.6**	45.8 ± 1.9**		
HBP-E	2.89 ± 0.33	989 ± 19.9	176 ± 12.4	36 ± 1.6	62.5 ± 8.1	1.52 ± 0.33
	2.01 ± 0.09*	900 ± 3.1*	201 ± 10.2*	36.2 ± 2.3*	38.2 ± 14.4*	1.47 ± 0.55*
	1.42 ± 0.05**	776 ± 17.8**	277 ± 8.1**	43.9 ± 1.9**		

[a] Note: * range of τ_M fixed between 750 and 900 ns during the fitting (IS + OS + SS). ** range of τ_M fixed between 750 and 900 ns during the fitting (IS + OS). The number of water molecules in the first coordination sphere (q) was fixed to 1, the distance between the Gd^{3+} and the innersphere water protons was set to 0.31 nm, the distance of the closest approach was fixed to 0.36 nm, the distance for the second sphere interaction was set to 0.36 nm and the diffusion coefficient was set to 2.9 10^{-9} m^2 s^{-1}. τ_{SO} is the electronic relaxation time at zero field, τ_V the correlation time modulating the electronic relaxation, τ_{SS} is the correlation time modulating the second sphere interaction and q_{SS} is the number of water molecules in the second sphere.

Several fittings were performed on each sample including: (i) IS + OS + SS contributions with τ_M allowed to vary from 500 ns to 1000 ns, (ii) IS + OS + SS contributions with τ_M allowed to vary from 750 ns to 900 ns, (iii) IS + OS contributions with τ_M allowed to vary from 500 ns to 1000 ns and (iv) IS + OS contributions with τ_M allowed to vary from 750 ns to 900 ns.

For CCS-A, a second sphere contribution was needed to obtain good agreement between the experimental and the fitted data whereas for CCS-B, the model with IS + OS gave good results and for CCS-C, addition of a second sphere contribution led to very low q_{SS} ($q_{SS} < 0.1$) indicating that this contribution is negligible. For the HBP samples, both types of fittings gave good results.

The fitted parameters show that as expected for a Gd-complex with an amide group complexing the Gd^{3+} ion, the water residence is quite long (750 to 1000 ns) and is quite similar for all samples. But the τ_R values are clearly dependent on the structure. CCS-A has the largest τ_R value indicating a poor flexibility of the Gd-complexes in this compound while for CCS-B, Gd-complexes seem to be rotating somewhat faster. The lowest τ_R value obtained for CCS-C could be explained by the reduced accessibility of water to the core which could lead to a lower water exchange rate. When τ_M was allowed to vary between 500 and 1500 ns during the fitting, a larger value of τ_R was obtained (0.74 ± 0.04 ns) with a τ_M equal to 1310 ± 44 ns. However this value of τ_R is still one order of magnitude lower than for CCS-A. For this type of compound with the Gd complexes in the core, it seems thus that some of the complexes are not accessible to water and thus not contribute to the observed relaxivity. Our results are in accord with the work reported on the functionalization of dendrimer surfaces using poly(ethylene glycol) (PEG) polymers; Kobayashi and co-workers[56] reported that the relaxivity of Gd^{3+}-dendrimer could be decreased by attaching a PEG layer around the dendrimer cores.

The rotational motion (τ_R) values derived from all of the polymeric nanostructures are very slow and much lower than for small molecule contrast agents (0.1 ns) resulting in a 3 to 6 fold increase of r_1 relaxivity at low field strengths (Table 4). In CCS-B nanoparticles where Gd is positioned in the star-arms and HBP-D and HBP-E nanoparticles, comparable values of τ_R are obtained. These τ_R values are in the optimal range for low magnetic field strengths, as shown by Caravan *et al.*[3,18,57] who performed simulations to understand the relative contributions of molecular parameters to longitudinal (r_1) and transverse (r_2) relaxivities as a function of the applied field. For example, Vasovist (MS-325) (an albumin-targeted intravascular contrast agent) displayed an increased relaxivity upon binding to albumin caused by a slower tumbling rate.[3] The positive effect of a slower rotational motion on the r_1 relaxivity disappeared at field strengths of 9.4 T consistent with the prediction of Caravan *et al.*[3] who showed that at very high field strengths an intermediate τ_R is more beneficial (0.5–4 ns). The nanoparticles built from star polymers provide a very versatile platform for studying the influence of the position of the Gd-complexes on the longitudinal relaxivity (r_1) of MRI contrast agents at different field strengths. Our results confirm that a low water exchange rate is a significant limiting factor in obtaining even higher relaxivity at all field strengths. The longitudinal relaxivity could be further improved by grafting Gd-complexes without amide function complexing the ion in order to increase the water exchange rate. Fig. S34 in the ESI† shows the relationship between the structure and the simulated relaxivity values using different τ_m and τ_R by Caravan *et al.*[3]

Conclusion

Complex polymeric architectures of functionalized P(OEGA) copolymers were synthesized as discrete single-macromolecule nanoparticle vectors for Gd ions, as MRI contrast agents.

Published on 18 December 2013. Downloaded by Fudan University on 21/01/2018 11:51:09.

Nanoparticles in the range 8–20 nm were easily prepared as MRI contrast agents. Our synthetic approach allowed us to tune the precise molecular placement of Gd ions within different localized environments inside the nanoparticles to allow optimization of MRI contrast at different magnetic field strengths. The relaxivity study confirms that that a low water exchange rate plays a key role in the relaxivity at high magnetic field strength.

Experimental part

Materials

N-Hydroxysuccinimide (98%), 2-bromopropionyl bromide (97%), carbon disulfide (≥99.9%), 1-butanethiol (99%), triethylamine (≥99.9%), poly(ethylene glycol) methyl ether acrylate (480 g mol^{-1}, 99%, OEGA), trifluoroacetic acid (99%), *N*,*N*′-bis(acryloyl)cystamine (>97%), *N*,*N*′-methylenebisacrylamide (≥99.5%), 1,6-hexanediol diacrylate (80%) and gadolinium(III) nitrate hexahydrate (99.99%) were purchased from Aldrich and used as received. Pentafluorophenyl acrylate (PFPA)[58] and 3-(trimethylsilyl)prop-2-yn-1-yl-2-(((((3-propionic acid)thio)carbonothioyl)thio)propanoate) (TSPPA)[32] were synthesized according to previously reported procedures. 2,2′-Azobis-(isobutyronitrile) (AIBN, Wako Chemicals) was crystallized twice from methanol before use. 1-(5-Amino-3-aza-2-oxopentyl)-4,7,10-tris-(*tert*-butoxycarbonylmethyl)-1,4,7,10-tetraazacyclododecane (DO3A–*t*Bu–NH_2, >94%) was purchased from Macrocyclics (Dallas, TX) and used as received. All solvents were purchased from Ajax Finechem, supplied at the highest purity available unless mentioned. High-purity N_2 (Linde gases) was used for degassing. Membranes for dialysis (MWCO 50 000 Da) were purchased from Fisher Biotec (CelluSepT4, regenerated cellulose tubular membrane).

Synthesis of 2,5-dioxopyrrolidin-1-yl-2-(((butylthio)-carbonothioyl)thio)propanoate (DPBP)

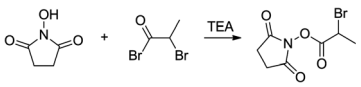

Synthesis of *N*-succinimidyl bromoacetate. *N*-Hydroxysuccinimide (4.03 g, 35 mmol) was dissolved in 50 ml dichloromethane (DCM) in a 250 ml round bottom flask equipped with a magnetic stir bar in an ice bath. Triethylamine (3.75 g, 37 mmol) in 10 ml DCM was added drop-wise to the solution. After stirring for 30 min, a solution of 2-bromopropionyl bromide (7.99 g, 37 mmol) in 10 DCM was added drop-wise over 1 hour. The resulting solution was stirred overnight at room temperature. The mixture was then washed with brine, and the organic phase was collected and dried over anhydrous magnesium sulfate. The solvent was removed by rotary evaporation and further dried in a vacuum oven at room temperature overnight, yielding a white powder. Yield 7.26 g (82.9%). ^{1}H NMR (300 MHz, $CDCl_3$) δ 4.57 (q, J = 7.0 Hz, 1H), 2.79 (s, 4H), 1.89 (d, J = 7.0 Hz, 3H) (Fig. S2 in the ESI†)

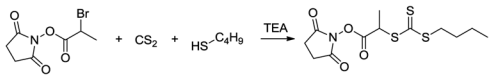

Synthesis of 2,5-dioxopyrrolidin-1-yl-2-(((butylthio)-carbonothioyl)thio)propanoate (DPBP). 1-Butanethiol (2.25 g, 25 mmol), carbon disulfide (1.9 g, 25 mmol) and 50 ml DCM were placed in a 250 ml round bottle flask equipped with a magnetic stir bar. After, triethylamine (5.06 g, 50 mmol) in 10 ml DCM was added drop-wise into the solution. The solution was left to stir at room temperature for 2 h and then *N*-succinimidyl bromoacetate (6.25 g, 25 mmol) in 10 ml DCM was added dropwise. The resulting solution was stirred overnight at room temperature. The final mixture was washed with a 0.1 M HCl aqueous solution (5 × 250 ml). Subsequently, the solvent was removed by rotary evaporation, and the product was purified by column chromatography using a mixture of ethyl acetate–petroleum spirit as eluent (1/50 v/v). The product was isolated by solvent evaporation and further dried in a vacuum oven at room temperature overnight to yield a yellow oil. Yield 5.53 g (65.9%). ^{1}H NMR (300 MHz, $CDCl_3$) δ 5.00 (q, J = 7.3 Hz, 1H), 3.54–3.26 (m, 2H), 2.98–2.75 (s, 4H), 1.74–1.63 (m, 2H), 1.62–1.50 (m, 3H), 1.48–1.30 (m, 2H), 1.00–0.85 (m, 3H) (Fig. S3 in the ESI†).

Synthesis of CCS-A

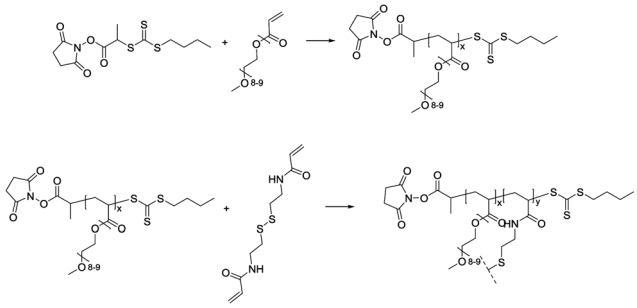

Synthesis of OEGA linear arm (Arm A). OEGA (0.96 g, 2 mmol), DPBP (23 mg, 0.07 mmol) and AIBN (1.2 mg, 0.007 mmol) were dissolved in acetonitrile (2 ml). The mixture was degassed by purging with N_2 for 30 min at 0 °C and was then placed in an oil bath at 60 °C. The polymerization was conducted for 8 h and then stopped by cooling the mixture in an ice bath and exposure to air. Monomer conversion was determined by ^{1}H NMR analysis and SEC analyses were undertaken to measure the molecular weight distributions. The polymer was purified by repeated precipitations in diethyl ether and then dried under vacuum. Yield 0.68 g (68.3%).

To make the star polymer, OEGA linear arm (0.5 g, 0.05 mmol, $\bar{M}_n$ = 10 000 g mol^{-1}, $Đ_m$ = 1.16), *N*,*N*′-bis(acryloyl)-cystamine (104 mg, 0.4 mmol), AIBN (2.5 mg, 0.015 mmol), and toluene (5 ml) were charged to a vial equipped with a magnetic stirrer. The mixture was purged with N_2 for 30 min at 0 °C, and then the polymerization was carried out at 70 °C for 24 h. After the polymerization, the vials were immediately cooled in an ice bath and the contents exposed to air. The polymer was purified by precipitation in tetrahydrofuran–petroleum spirit (1/1 v/v)

 This journal is © The Royal Society of Chemistry 2014

Published on 18 December 2013. Downloaded by Fudan University on 21/01/2018 11:51:09.

and then dried under vacuum. Yield 0.56 g (92.4%). The final composition determined by ^{1}H NMR is equal to 89/11 mol% in OEGA and NHS ester (Fig. S1, S4 and S9 in the ESI†).

Synthesis of CCS-B

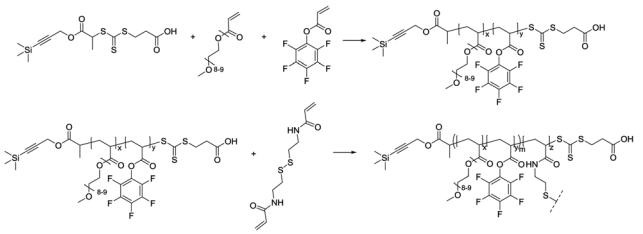

Synthesis of P(OEGA-*stat*-PFPA) linear arm (Arm B). OEGA (0.96 g, 2 mmol), PFPA (202 mg, 0.85 mmol), TSPPA (40 mg, 0.11 mmol), and AIBN (1.8 mg, 0.01 mmol) were dissolved in acetonitrile (2.8 ml). The mixture was degassed by purging with N_2 for 30 min at 0 °C and then placed in an oil bath at 60 °C. The polymerization was conducted for 8 h and then stopped by cooling the mixture in an ice bath and exposure to air. Monomer conversion was determined by ^{1}H and ^{19}F NMR and SEC analyses were undertaken to measure the molecular weight distribution. The polymer was purified by repeated precipitations in diethyl ether and then dried under vacuum. Yield 1.02 g (84.8%).

To prepare the star polymer, OEGA-stat-PFPA linear arm (0.45 g, 0.05 mmol, $\bar{M}_n$ = 9000 g mol^{-1}, $Đ_m$ = 1.14), *N*,*N*′-bis(acryloyl)cystamine (104 mg, 0.4 mmol), AIBN (2.5 mg, 0.015 mmol), and toluene (5 ml) were charged to a vial equipped with a magnetic stirrer. The mixture was purged with N_2 for 30 min at 0 °C, and then the polymerization was carried out at 70 °C for 24 h. After the polymerization, the vials were immediately cooled in an ice bath and the contents exposed to air. The polymer was purified by precipitation in tetrahydrofuran–petroleum spirit (1/1 v/v) and then dried under vacuum. Yield 0.52 g (93.9%). The final composition was determined by ^{1}H NMR and ^{19}F NMR and was equal to 80/20 mol% in OEGA and PFPA (Fig. S1, S5, S6, S10 and S11 in the ESI†).

Synthesis of CCS-C

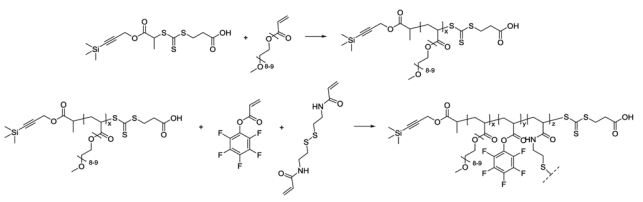

Synthesis of OEGA linear arm (Arm C). OEGA (0.96 g, 2 mmol), TSPPA (25 mg, 0.07 mmol) and AIBN (1.3 mg, 0.008 mmol) were dissolved in acetonitrile (2 ml). The mixture was degassed by purging with N_2 for 30 min at 0 °C and then placed in an oil bath at 60 °C. The polymerization was conducted for 8 h and then stopped by cooling the mixture in an ice bath and exposure to air. Monomer conversion was determined by ^{1}H NMR and SEC analyses were undertaken to measure the molecular weight distribution. The polymer was purified by repeated precipitations in diethyl ether and then dried under vacuum. Yield 0.75 g (76%).

OEGA linear arm (550 mg, 0.05 mmol, $\bar{M}_n$ = 11 000 g mol^{-1}, $Đ_m$ = 1.14), PFPA monomer (369 mg, 1.55 mmol), *N*,*N*′-bis-(acryloyl)cystamine (104 mg, 0.4 mmol), AIBN (3 mg, 0.018 mmol), and toluene (5 ml) were charged to a vial equipped with a magnetic stirrer. The mixture was purged with N_2 for 30 min at 0 °C, and then the polymerization was carried out at 70 °C for 24 h. After the polymerization, the vials were immediately cooled in an ice bath and the contents exposed to air. The polymer was purified by precipitation in tetrahydrofuran–petroleum spirit (1/1 v/v) and then dried under vacuum. Yield 0.90 g (87.9%). The final composition determined by ^{1}H NMR and ^{19}F NMR is equal to 60/40 mol% in OEGA and PFPA (Fig. S1, S7, S8, S12 and S13 in the ESI†).

Synthesis of HBP-D

Synthesis of hyperbranched P(OEGA-*co*-PFPA). OEGA (5 g, 4.59 ml, 10 mmol), PFPA (620 mg, 2.6 mmol), *N*,*N*′-methylenebisacrylamide (199 mg, 1.29 mmol), TSPPA (250 mg, 0.78 mmol) and AIBN (8.5 mg, 0.052 mmol) were dissolved in acetonitrile (13 ml) and the mixture was purged with N_2 for 30 min at 0 °C. The solution was stirred at 60 °C for 24 h and the polymerization was then stopped by cooling it in an ice bath. Aliquots were taken to determine the monomer conversion by ^{1}H & ^{19}F NMR and molecular weight by SEC. The polymer was purified by repeated precipitations in cold diethyl ether and then dried under vacuum. The final composition determined by ^{1}H NMR and ^{19}F NMR is equal to 75/25 mol% in OEGA and PFPA (Fig. S14 and S15 in the ESI†).

Synthesis of HBP-E

Synthesis of hyperbranched P(OEGA-*co*-PFPA). OEGA (5 g, 4.59 ml, 10 mmol), PFPA (620 mg, 2.6 mmol), 1,6-hexanediol diacrylate (292 mg, 1.29 mmol), TSPPA (250 mg, 0.78 mmol) and AIBN (8.5 mg, 0.052 mmol) were dissolved in acetonitrile (13 ml) and the mixture was purged with N_2 for 30 min at 0 °C. The solution was stirred at 60 °C for 24 h and the polymerization was then stopped by cooling it in an ice bath. Aliquots were taken to determine the monomer conversion *via* ^{1}H and ^{19}F NMR and molecular weight by SEC. The polymer was purified by repeated precipitations in cold diethyl ether and then dried under vacuum. The final composition determined by ^{1}H NMR and ^{19}F NMR is equal to 76/24 mol% in OEGA and PFPA (Fig. S16 and S17 in the ESI†).

Chemical modification with DO3A–*t*Bu–NH_2 chelate and deprotection

A typical procedure for the chemical modification of active esters (PFP and NHS esters) with DO3A–*t*Bu–NH_2 is given as follows: star polymer (0.2 mmol of active ester functionality) was dissolved in DMF (2 ml). DO3A–*t*Bu–NH_2 (153 mg, 0.22 mmol)

Published on 18 December 2013. Downloaded by Fudan University on 21/01/2018 11:51:09.

and triethylamine (22 mg, 0.22 mmol) were added, and the mixture was stirred for 48 h. The polymer was purified by several precipitations in diethyl ether and then analyzed by ^{1}H NMR and ^{19}F NMR spectroscopy. The solvent was evaporated, trifluoroacetic acid 2 ml was added, and the deprotection reaction was carried out overnight at room temperature. Then, unreacted TFA was removed by evaporation and the polymer was further purified by dialysis using a membrane with a molecular weight cutoff 50 000 Da for 3 days against water. The star polymer was recovered as a yellowish tacky solid after freeze-drying (Fig. S18–S26 in the ESI†).

Complexation with Gd^{3+}

The star polymer with DO3A moieties was dissolved in water, the pH was adjusted to 6, and the solution was heated at 60 °C for 1 h. $Gd(NO_3)_3 \cdot 6H_2O$ (1.5 eq.) was added, the pH was adjusted to 8, and the mixture was stirred for 48 h at room temperature. DOTA was then added to the aqueous solution to remove unreacted Gd^{3+} ions; the polymer was dialyzed against water for 5 days and freeze-dried. The final Gd^{3+} content was assessed using inductively coupled plasma optical emission spectrometry (ICP-OES).

Analyses

NMR spectroscopy. Polymer compositions were assessed by ^{1}H and ^{19}F NMR using a Bruker AC300F (300 MHz) spectrometer or a Bruker DPX300 (300 MHz) spectrometer.

Size exclusion chromatography (SEC). SEC analyses of polymer samples were performed in *N*,*N*-dimethylacetamide (DMAc) with 0.03% w/v LiBr and 0.05% 2,6-dibutyl-4-methylphenol (BHT) using a Shimadzu modular system comprising a DGU-12A degasser, an SIL-10AD automatic injector, and a 5.0 μm bead-size guard column (50 × 7.8 mm) followed by four 300 × 7.8 mm linear Phenogel columns (bead size: a 5.0 μm; pore sizes: 105, 104, 103, and 500 Å) and an RID-10A differential refractive-index detector. The temperature of columns was maintained at 50 °C using a CTO-10A oven, and the flow rate was kept at 1 ml min^{-1} using an LC-10AT pump. A molecular weight calibration curve was produced using commercial narrow molecular weight distribution polystyrene standards with molecular weights ranging from 500 to 10^6 g mol^{-1}. Polymer solutions at 2–3 mg ml^{-1} were prepared in the eluent and filtered through 0.45 μm filters prior to injection.

Dynamic light scattering (DLS). DLS measurements were performed using a Malvern Zetasizer Nano Series running DTS software and using a 4 mW He–Ne laser operating at a wavelength of 633 nm and an avalanche photodiode (APD) detector. The scattered light was detected at an angle of 173°. The temperature was stabilized to ±0.1 °C of the set temperature. Aqueous solutions of polymer samples were filtered through a 0.45 μm pore size filter to remove dust prior to measurement. To assess size distributions, the autocorrelation function was fitted using the cumulants method.

Inductively coupled plasma-optical emission spectrometry (ICP-OES). The Gd^{3+} content of the macromolecular CAs was determined by inductively coupled plasma-optical emission spectrometry (ICP-OES) using a Perkin-Elmer OPTIMA 7300 spectrometer. Samples were prepared by dissolving 0.5 mg of polymer in 10 ml of ultrapure water.

Relaxivity measurements. ^{1}H NMRD curves (nuclear magnetic resonance dispersion) of the macromolecular CAs were obtained at 310 K on a Stelar fast cycling relaxometer (PV, Mede, Italy) over a range of magnetic fields extending from 0.25 mM to 0.94 T (0.01–40 MHz). Measurements of T_1 and T_2 relaxation times were performed at 310 K on Minispec Mq-20 and Mq-60 (Bruker, Karlsruhe, Germany) working at 20 MHz (0.47 T) and 60 MHz (1.4 T), respectively. Furthermore, measurements at very high magnetic field were performed on a 9.4 T Biospin 94/20 USR (Bruker, Karlsruhe, Germany) equipped with a Transceiver RES ^{1}H 72 mm Quad RF coil. T_1 relaxation times were acquired using a Rapid Acquisition Rapid Echo with Variable Repetition Time (RARE-VTR) sequence, whereas T_2 relaxation times were obtained using a Multi-Slice-Multi-Echo (MSME) sequence.

Acknowledgements

The authors acknowledge the Australian Research Council (ARC) for funding in the form of a Discovery grant (DP110104251). In addition, we would like to acknowledge a significant research fellowship funding from ARC to CB (Future Fellowship (ARC-FT 120100096) and ARC-APD Fellowship) and to ABL (ARC-FT110100046). This work was supported by the ARC Programs of the French Community of Belgium, UIAP VII and the FNRS (Fond National de la Recherche Scientifique). The support and sponsorship provided by COST Action TD1004. The authors thank the Center for Microscopy and Molecular Imaging (CMMI), supported by the European Regional Development Fund and the Walloon Region.

Notes and references

1 P. Hermann, J. Kotek, V. Kubicek and I. Lukes, *Dalton Trans.*, 2008, 3027–3047.
2 E. J. Werner, A. Datta, C. J. Jocher and K. N. Raymond, *Angew. Chem., Int. Ed.*, 2008, **47**, 8568–8580.
3 P. Caravan, J. J. Ellison, T. J. McMurry and R. B. Lauffer, *Chem. Rev.*, 1999, **99**, 2293–2352.
4 C. Boyer, M. R. Whittaker, V. Bulmus, J. Liu and T. P. Davis, *NPG Asia Mater.*, 2010, **2**, 23–30.
5 S. Laurent, D. Forge, M. Port, A. Roch, C. Robic, L. Vander Elst and R. N. Muller, *Chem. Rev.*, 2008, **108**, 2064–2110.
6 M. Mahmoudi, H. Hosseinkhani, M. Hosseinkhani, S. Boutry, A. Simchi, W. S. Journeay, K. Subramani and S. Laurent, *Chem. Rev.*, 2010, **111**, 253–280.
7 J. Gao, H. Gu and B. Xu, *Acc. Chem. Res.*, 2009, **42**, 1097–1107.
8 H. B. Na, I. C. Song and T. Hyeon, *Adv. Mater.*, 2009, **21**, 2133–2148.
9 E. Terreno, D. D. Castelli, A. Viale and S. Aime, *Chem. Rev.*, 2010, **110**, 3019–3042.
10 C. F. G. C. Geraldes and S. Laurent, *Contrast Media Mol. Imaging*, 2009, **4**, 1–23.

 This journal is © The Royal Society of Chemistry 2014

Published on 18 December 2013. Downloaded by Fudan University on 21/01/2018 11:51:09.

11 S. Aime, M. Botta and E. Terreno, in *Advances in Inorganic Chemistry*, Academic Press, 2005, pp. 173–237.
12 S. Aime, E. Gianolio, E. Terreno, G. B. Giovenzana, R. Pagliarin, M. Sisti, G. Palmisano, M. Botta, M. P. Lowe and D. Parker, *JBIC, J. Biol. Inorg. Chem.*, 2000, **5**, 488–497.
13 M. A. Perazella, *Clin. J. Am. Soc. Nephrol.*, 2009, **4**, 461–469.
14 N. Bloembergen, *J. Chem. Phys.*, 1957, **27**, 572–573.
15 N. Bloembergen and L. O. Morgan, *J. Chem. Phys.*, 1961, **34**, 842.
16 N. Bloembergen, E. M. Purcell and R. V. Pound, *Phys. Rev.*, 1948, **73**, 679–712.
17 I. Solomon, *Phys. Rev.*, 1955, **99**, 559–565.
18 P. Caravan, *Chem. Soc. Rev.*, 2006, **35**, 512–523.
19 S. Aime, D. D. Castelli, S. G. Crich, E. Gianolio and E. Terreno, *Acc. Chem. Res.*, 2009, **42**, 822–831.
20 A. J. L. Villaraza, A. Bumb and M. W. Brechbiel, *Chem. Rev.*, 2010, **110**, 2921–2959.
21 G. Adam, J. Neuerburg, E. Spüntrup, A. Mühler, K. S. V. Surg and R. W. Günther, *J. Magn. Reson. Imag.*, 1994, **4**, 462–466.
22 B. Zarabi, A. Nan, J. Zhuo, R. Gullapalli and H. Ghandehari, *Mol. Pharmaceutics*, 2006, **3**, 550–557.
23 K. Shiraishi, K. Kawano, Y. Maitani and M. Yokoyama, *J. Controlled Release*, 2010, **148**, 160–167.
24 K. Shiraishi, K. Kawano, T. Minowa, Y. Maitani and M. Yokoyama, *J. Controlled Release*, 2009, **136**, 14–20.
25 M. Grogna, R. Cloots, A. Luxen, C. Jerome, C. Passirani, N. Lautram, J.-F. Desreux and C. Detrembleur, *Polym. Chem.*, 2010, **1**, 1485–1490.
26 T. Liu, Y. Qian, X. Hu, Z. Ge and S. Liu, *J. Mater. Chem.*, 2012, **22**, 5020–5030.
27 X. Li, Y. Qian, T. Liu, X. Hu, G. Zhang, Y. You and S. Liu, *Biomaterials*, 2011, **32**, 6595–6605.
28 H. Kobayashi and M. W. Brechbiel, *Adv. Drug Delivery Rev.*, 2005, **57**, 2271–2286.
29 S. Langereis, A. Dirksen, T. M. Hackeng, M. H. P. van Genderen and E. W. Meijer, *New J. Chem.*, 2007, **31**, 1152–1160.
30 K. Nwe, L. H. Bryant and M. W. Brechbiel, *Bioconjugate Chem.*, 2010, **21**, 1014–1017.
31 C. T. Adkins, J. N. Dobish, C. S. Brown, B. Mayrsohn, S. K. Hamilton, F. Udoji, K. Radford, T. E. Yankeelov, J. C. Gore and E. Harth, *Polym. Chem.*, 2012, **3**, 390–398.
32 Y. Li, M. Beija, S. Laurent, L. V. Elst, R. N. Muller, H. T. T. Duong, A. B. Lowe, T. P. Davis and C. Boyer, *Macromolecules*, 2012, **45**, 4196–4204.
33 K. Khanna, S. Varshney and A. Kakkar, *Polym. Chem.*, 2010, **1**, 1171–1185.
34 C. Zhang, M. Miao, X. Cao and Z. An, *Polym. Chem.*, 2012, **3**, 2656–2664.
35 Q. Qiu, G. Liu and Z. An, *Chem. Commun.*, 2011, **47**, 12685–12687.
36 Q. Chen, X. Cao, Y. Xu and Z. An, *Macromol. Rapid Commun.*, 2013, **34**, 1507–1517.
37 A. Blencowe, J. F. Tan, T. K. Goh and G. G. Qiao, *Polymer*, 2009, **50**, 5–32.
38 K. J. Thurecht, I. Blakey, H. Peng, O. Squires, S. Hsu, C. Alexander and A. K. Whittaker, *J. Am. Chem. Soc.*, 2010, **132**, 5336–5337.
39 J. T. Wiltshire and G. G. Qiao, *Macromolecules*, 2006, **39**, 9018–9027.
40 A. P. Vogt, S. R. Gondi and B. S. Sumerlin, *Aust. J. Chem.*, 2007, **60**, 396–399.
41 C. Boyer, V. Bulmus, T. P. Davis, V. Ladmiral, J. Liu and S. Perrier, *Chem. Rev.*, 2009, **109**, 5402–5436.
42 C. Boyer, M. H. Stenzel and T. P. Davis, *J. Polym. Sci., Part A: Polym. Chem.*, 2011, **49**, 551–595.
43 M. H. Lee, Z. Yang, C. W. Lim, Y. H. Lee, S. Dongbang, C. Kang and J. S. Kim, *Chem. Rev.*, 2013, **113**, 5071–5109.
44 J. Ferreira, J. Syrett, M. Whittaker, D. Haddleton, T. P. Davis and C. Boyer, *Polym. Chem.*, 2011, **2**, 1671–1677.
45 J. A. Syrett, D. M. Haddleton, M. R. Whittaker, T. P. Davis and C. Boyer, *Chem. Commun.*, 2011, **47**, 1449–1451.
46 M. Bathfield, F. D'Agosto, R. Spitz, M.-T. Charreyre and T. Delair, *J. Am. Chem. Soc.*, 2006, **128**, 2546–2547.
47 J. Liu, H. Duong, M. R. Whittaker, T. P. Davis and C. Boyer, *Macromol. Rapid Commun.*, 2012, **33**, 760–766.
48 M. Luzon, C. Boyer, C. Peinado, T. Corrales, M. Whittaker, L. Tao and T. P. Davis, *J. Polym. Sci., Part A: Polym. Chem.*, 2010, **48**, 2783–2792.
49 B. Liu, A. Kazlauciunas, J. T. Guthrie and S. Perrier, *Macromolecules*, 2005, **38**, 2131–2136.
50 J. Rosselgong and S. P. Armes, *Macromolecules*, 2012, **45**, 2731–2737.
51 C. F. G. C. Geraldes, A. D. Sherry, R. D. Brown and S. H. Koenig, *Magn. Reson. Med.*, 1986, **3**, 242–250.
52 S. Aime, M. Botta, M. Fasano and E. Terreno, *Acc. Chem. Res.*, 1999, **32**, 941–949.
53 M. Grogna, R. Cloots, A. Luxen, C. Jerome, J.-F. Desreux and C. Detrembleur, *J. Mater. Chem.*, 2011, **21**, 12917–12926.
54 D. A. Fulton, M. O'Halloran, D. Parker, K. Senanayake, M. Botta and S. Aime, *Chem. Commun.*, 2005, 474–476.
55 R. N. Muller, L. V. Elst, P. A. Rinck, P. Vallet, F. Maton, H. Fischer, A. Roch and Y. V. Haverbeke, *Invest. Radiol.*, 1988, **23**, S229–S231.
56 C. Kojima, B. Turkbey, M. Ogawa, M. Bernardo, C. A. S. Regino, L. H. Bryant, Jr, P. L. Choyke, K. Kono and H. Kobayashi, *Nanomedicine*, 2011, **7**, 1001–1008.
57 P. Caravan, C. T. Farrar, L. Frullano and R. Uppal, *Contrast Media Mol. Imaging*, 2009, **4**, 89–100.
58 C. Boyer and T. P. Davis, *Chem. Commun.*, 2009, 6029–6031.